

TUMOR PROGRESSION AND PHARMACOLOGICAL INTERVENTION: MODELING IMMUNOTHERAPEUTIC AND CHEMOTHERAPY STRATEGIES IN NEUROBLASTOMA

Kate Brockman², Brian Colburn¹, Joseph Garza³, Yidong Liao¹, and BV Shankara Narayana Rao¹

¹*Department of Mathematics and Statistics, Texas A&M University - Corpus Christi*

²*Department of Engineering, Texas A&M University - Corpus Christi*

³*Department of Life Sciences, Texas A&M University - Corpus Christi*

Abstract. Neuroblastoma, one of the most common solid cancerous tumors found in children is one of the leading causes of childhood cancer. Despite advancements in treatment, there is still an ongoing need for optimal therapy strategies and more accurate mathematical models to guide clinical decision-making for neuroblastoma patients. Among available treatments, immunotherapy and chemotherapy, particularly the use of Interleukin-2 (IL-2) and Cyclophosphamide, have shown encouraging results by enhancing the immune-response and targeting cancerous cells. Therefore, in this study we developed a nonlinear system of coupled first-order differential equations to simulate the interactions between tumor cells, natural killer (NK) cells, and cytotoxic T lymphocytes (CTLs). The model accounted for the effects of IL-2 and Cyclophosphamide on these immune cell populations, by examining tumor dynamics across different patient risk groups. The resulting framework provides a theoretical approach to optimizing therapeutic strategies and improving clinical outcomes in neuroblastoma treatment.

1. Introduction. Cancer is characterized as a disease associated by the uncontrolled proliferation of abnormal cells. These cells invade and disrupt surrounding healthy tissue and have been proved to be caused by a combination of genetic predispositions, environmental exposures, and lifestyle related factors [15]. Neuroblastoma, holds a significant place in pediatric oncology due to its high prevalence in children with development occurring most commonly in infants within their first year of life, which may present as either localized or widespread metastatic disease [16]. Clinically, patients are classified into various risk categories outlined by the International Neuroblastoma Risk Group (INRG). For this study, we stratified patient populations into three groups: low, intermediate, and high, based on this existing framework (Table 1), which takes into account factors such as age, tumor stage, histology, and genetic components. For low-risk patients, who have an estimated survival rate above 98%, observation or surgical resection is usually sufficient for tumor reduction. Intermediate-risk patients with survival rates exceeding 90%, often receive chemotherapy in combination with surgery. In contrast, high-risk patients undergo a multi-faceted approach that includes multiple cycles of chemotherapy, surgical resection, radiation and immunotherapy [2]. This standardized risk-differentiated patient classification system facilitates better survival outcomes by providing an objective framework to optimize treatment strategies in neuroblastoma, whilst minimizing long-term adverse effects of the treatment. Given the increasing use of immunotherapies in treatment regimens, a deeper understanding of the immune system's role in tumor control has now become essential [1].

Biologically, the immune response in human bodies can be broken up into a two-part system: the innate and adaptive immune systems; each contributing uniquely to tumor recognition and elimination. In this study, NK cells were modeled in association with the innate immune system, representing rapid and non-specific responses to cancerous cells. CTLs, in contrast, were associated with the adaptive immune system with cell that assemble antigen-specific responses following activation and clonal expansion [8]. This differentiation is central to the development of an immunotherapeutic framework, as it reflects the differences in cell activation timing and therapeutic targeting in human bodies. By incorporating both NK cells and CTLs into the presented pharmacology model, we capture the complementary roles of innate and adaptive immunity in shaping tumor-immune dynamics under various treatment conditions. These differences formed the foundation for simulating immune responses across various patient categories and treatment protocols.

Historically, mathematical modeling has played an important role in cancer research, bridging the gap between theoretical biology and clinical applications [3-5,7,10,13,17]. As our collective biological understanding of cancer has increased, mathematical and computational models have become essential tools for integrating diverse data types and biological processes into frameworks capable of simulating the treatment outcomes of cancer patients [13]. In the context of neuroblastoma, models such as the one developed offer valuable insights into tumor progression, therapeutic response, and theoretical disease evolution. They support a wide range of applications, including the optimization of chemotherapy scheduling, immunotherapy planning, and personalized treatment strategies. Furthermore, these models enable the formulation of testable hypotheses and the incorporation of experimental and clinical data into predictive simulations [13]. However, despite their promise, oncological modeling is challenged by the inherent complexity of biological systems and the rigorous demands of model validation, verification, and clinical integration.

2. Model. Building on a previously established framework by Song [17], this study modeled the cellular interactions between tumor cells, NK cells, and CTLs, with additions to incorporate the therapeutic effects of two

drugs used for the treatment of neuroblastoma.

2.1. Objective pharmacology model. The pharmacology model developed showed the immune tumor dynamics of neuroblastoma progression and evaluated its therapeutic effects by incorporating immunotherapy and chemotherapy treatments. The model (Equation 2.1) integrated key biological processes including tumor growth, immune activation, and drug-induced modulation of immune responses.

$$(2.1) \quad \begin{cases} N'(t) = a_1 N(t)(1 - bN(t)) - a_2 N(t) - \alpha_1 N(t)T(t) + k_i I(t) \\ L'(t) = r_1 N(t)T(t) - \mu L(t) - \beta_1 L(t)T(t) \\ T'(t) = cT(t)(1 - dT(t)) - \alpha_2 N(t)T(t) - \beta_2 L(t)T(t) - k_c C(t) \\ I'(t) = -\frac{\log(2)}{h_i} 2^{-\frac{t}{h_i}} I(0) \\ C'(t) = -\frac{\log(2)}{h_c} 2^{-\frac{t}{h_c}} C(0) \end{cases}$$

Let $N(t)$, $L(t)$, and $T(t)$ represent the populations of NK cells, CTLs, and tumor cells, while $I(t)$ and $C(t)$ denote the concentrations of IL-2 and Cyclophosphamide.

2.2. Nondimensionalization. To reduce model complexity and highlight biological mechanisms, the system was nondimensionalized (Equation 2.2) using appropriate scaling transformations based on characteristic population sizes and rates. This approach reformulates the equations in terms of dimensionless variables and parameters, allowing for a more straightforward interpretation and comparison across treatment groups.

$$(2.2) \quad \begin{cases} N'(t) = p_1 N(t)(1 - qN(t)) - p_2 N(t) - N(t)T(t) + k_i I(t) \\ L'(t) = N(t)T(t) + rD(t) - L(t) - sL(t)T(t) \\ T'(t) = uT(t)(1 - vT(t)) - N(t)T(t) - \delta L(t)T(t) - k_c C(t) \\ I'(t) = -\frac{\log(2)}{h_i} 2^{-\frac{t}{h_i}} I(0) \\ C'(t) = -\frac{\log(2)}{h_c} 2^{-\frac{t}{h_c}} C(0) \end{cases}$$

The simplification brings about parameters $p_1 = \frac{a_1}{\mu}$ and $p_2 = \frac{a_2}{\mu}$, which normalize the NK cell proliferation and natural death rates relative to the CTL death rate μ . The parameter $q = \frac{b}{\mu\alpha_2}$ represents the NK cell carrying capacity scaled by the NK-induced tumor cell death rate. The term $r = \frac{T(0)}{\alpha_1\alpha_2} \cdot \frac{r_1}{\mu}$ accounts for CTL activation resulting from tumor cell byproducts generated by NK induced cytotoxicity, scaled by the initial tumor burden. The parameter $s = \frac{\beta_1}{\alpha_1}$ expresses the relative rates at which CTLs and NK cells are lost through interactions with tumor cells. The tumor growth rate is scaled as $u = \frac{c}{\mu}$, and the term $v = \frac{du}{\alpha_1}$ captures the effects of tumor carrying capacity modulated by NK activity. Finally, $\delta = \frac{\beta_2 r_1}{\alpha_1\alpha_2}$ characterizes the CTL-induced tumor cell death rate relative to that of NK cells. Together, these nondimensionalized parameters (Table X) highlight the dominant mechanisms governing tumor-immune dynamics and enable a more generalized analysis across treatments and patient disease profiles.

3. Methods.

3.1. Numerical Methods. Numerical simulations were performed in Python using the `SciPy` library. Parameter values were adapted from existing literature (Table 3), while initial immune and tumor cell counts were determined based on relative proportions characteristic of each neuroblastoma risk group (Table 2). Simulations were run across the three patient-risk categories to assess immune response dynamics and treatment effectiveness under varying clinical conditions.

3.2. Mathematical Methods. The mathematical method includes the overview of the Caputo fractional order derivative and how it will apply to the system of differential equations from (2.2).

3.2.1. Caputo Fractional Order Derivative Framework. To enhance the biological nature of our neuroblastoma model, we incorporated a Caputo fractional-order derivative to capture tumor dynamics. This framework applied to three the differential equations representing CTL, NK, and Tumor cells, excluding the drug/treatment variables of Cyclophosphamide (C) and Interleukin-2 (IL-2). The Cyclophosphamide and Interleukin-2 concentrations can be assumed to be 0 so that Equations from (2.2) may be operated on. The Caputo Operator facilitated

improved accuracy of tumor growth modeling by accounting for past system behavior, as demonstrated in recent studies [10]

Tumor cells, CTLs, and NK cells are denoted by T, L, and N, respectively. All other parameters are defined in Table 3.

Definition 1: Consider the following function $\varphi(t)$, when $t > 0$, and the Riemann-Liouville Integral (RLI) operator of a function $\varphi(t)$ is defined as follows:

$$(3.1) \quad I^\alpha \varphi(t) = \int_0^t \frac{(t-\tau)^{\alpha-1}}{\Gamma(\alpha)} \varphi(\tau) d\tau$$

$\alpha > 0$ is the order derivative.

The fractional derivative operator is denoted D_0^α and $\alpha > 0$ defines the fractional order allowing to model memory and hereditary effects better than the classical integer order derivatives when $\alpha > 0$ lies between the integer values and the gamma function are the generalization of the factorial function to continuous values, and $(t-\tau)^{\alpha-1}$ is the kernel function that is being integrated and gives the fractional derivative its memory property, where τ is a past time point on the interval $[0, t]$.

The fractional-order derivative of function $\varphi(t)$ in [equation 1] is defined by the following:

$$(3.2) \quad D^\alpha \varphi(t) = I^{n-\alpha} D^{(n)} \varphi(t)$$

where $D = d/dt$

Definition 2: Consider the function $\varphi(t)$ when $t > 0$, the Caputo fractional derivative of order α when $\alpha > 0$ is given by the following:

$$(3.3) \quad D^\alpha \varphi(t) = \frac{1}{\Gamma(n-\alpha)} \int_0^t (t-\tau)^{n-\alpha-1} \varphi^{(n)}(\tau) d\tau$$

where n is an integer, and $\alpha \in (n-1, n)$ and $D^\alpha \varphi(t)$ is the Caputo fractional operator of the function $\varphi(t)$.

Theorem 1: Consider a system of fractional order equations in the form:

$$(3.4) \quad D_0^\alpha \varphi(t) = \varphi(t, Y(t)), Y(t_0) = Y_0$$

The following statements will be true when $J(Y^*)$ is the Jacobian Matrix:

- The equilibrium point is asymptotically stable only if all eigenvalues of the Jacobian Matrix satisfy $\arg \lambda_i > a\pi/2$ from 3.19 and 3.20
- The equilibrium point is unstable only if all eigenvalues of the Jacobian Matrix such that $\arg \lambda_i < a\pi/2$ from 3.19 and 3.20

Here we generalize an integer-order tumor interaction model, given by the following equations (3.5)–(3.7) is a set that is a continuous nonlinear ordinary differential equation:

$$(3.5) \quad N'(t) = \alpha_1 N(t)(1 - bN(t)) - \alpha_2 N(t) - \alpha_1 N(t)T(t)$$

$$(3.6) \quad L'(t) = r_1 N(t)T(t) + r_2 D(t) - \mu L(t) - \beta_1 L(t)T(t)$$

$$(3.7) \quad T'(t) = cT(t)(1 - dT(t)) - \alpha_2 N(t)T(t) - \beta_2 L(t)T(t)$$

where N , L , and T represent the populations of the natural killer (NK) cells, cytotoxic t lymphocytes, and tumor (T) cells respectively. Furthermore α_1 , α_2 , b , r_1 , r_2 , μ , β_1 , β_2 , and c are all parameters from Table 3.

After non-dimensionalizing equations (3.5)–(3.7), we get the following equations:

$$(3.8) \quad N'(t) = p_1 N(t)(1 - qN(t)) - p_2 N(t) - N(t)T(t)$$

$$(3.9) \quad L'(t) = N(t)T(t) + rD(t) - L(t) - sL(t)T(t)$$

$$(3.10) \quad T'(t) = uT(t)(1 - vT(t)) - N(t)T(t) - (\delta)L(t)T(t)$$

where p_1, p_2, q, r, s, u, v , and δ are the nondimensional parameters. Now the proposed dimensionless model is put into Caputo fractional order derivative form with the following equations:

$$(3.11) \quad D_0^\alpha x(t) = p_1x(t)(1 - qx(t)) - p_2x(t)z(t)$$

$$(3.12) \quad D_0^\alpha y(t) = x(t)z(t) + rd(t) - y(t) - sy(t)z(t)$$

$$(3.13) \quad D_0^\alpha z(t) = uz(t)(1 - vz(t)) - x(t)z(t) - \delta y(t)z(t)$$

when $\alpha > 0$ is the order derivative, and $x(t)$, $y(t)$, and $z(t)$ represent the respective cell populations of the NK cells, CTLs, and T cells.

In this section, a lemma and definitions will prove the existence of a unique solution of the fractional order tumor model.

Lemma 1: Consider the system of equations defined by Caputo fractional-order derivatives:

$$(3.14) \quad D^a x(t) = p_1x(1 - qx) - p_2xz$$

$$(3.15) \quad D^a y(t) = xz + rd - y - syz$$

$$(3.16) \quad D^a z(t) = uz(1 - vz) - xz - \delta yz$$

where $0 < a \leq 1$. Then the system admits a unique solution under appropriate conditions, ensuring that disturbances in initial conditions do not lead to non-deterministic behaviors. This reinforces the stability of the fractional-order system.

The initial conditions of the fractional order derivatives can be written as $x(t_0) = x_0, y(t_0) = t_0$, and $z(t_0) = z_0$. Equations (3.11)–(3.13) can be written in the form:

$$(3.17) \quad D^a Y(t) = R_1 Y(t) + x(t)R_2 Y(t), Y(t_0) = Y_0$$

where Y_0 are initial conditions of the function $Y(t)$ which is the column vector of the equations $x(t)$, $y(t)$, and $z(t)$ are the respective population equations of natural killer cells, cytotoxic t-lymphocyte cells, and tumor cells

$$(3.18) \quad Y(t) = \begin{bmatrix} x(t) \\ y(t) \\ z(t) \end{bmatrix}$$

$$(3.19) \quad R_1 = \begin{bmatrix} 0 & 0 & 0 \\ 0 & -1 & 0 \\ u & 0 & v \end{bmatrix}$$

$$(3.20) \quad R_2 = \begin{bmatrix} p_1(1 - q) & 0 & -p_2 \\ 1 & 0 & 0 \\ -1 & -\delta & -1 \end{bmatrix}$$

The following definitions are required for the existence and uniqueness of solutions for equation 3.17 .

Definition 3: Consider $C[0, \theta]$ to belong to a continuous vector $Y(t)$ with the components of functions of $x(t)$, $y(t)$, and $z(t)$

Definition 4: $Y(t)$ is a column vector that satisfies equation (3.20) which belongs to $C[0, \theta]$.

Theorem 2: The system of equations given by equation (3.20) has a unique solution $Y(t)$ that belongs to $C[0, \theta]$

Proof of Lemma 1: The system of fractional order differential equations (3.14)-(3.16) can be written as follows:

$$(3.21) \quad I^{1-a} \frac{d}{dt} Y(t) = R_1 Y(t) + x(t) R_2 Y(t)$$

where

$$(3.22) \quad D_\alpha[Y] = I^{1-a} \frac{d}{dt} Y(t)$$

$R_1 Y(t)$ indicates that $Y(t)$ evolves with a rate proportional to itself (logistic/ exponential growth/decay)
 $x(t) R_2 Y(t)$ introduces the interaction between $y(t)$ and $x(t)$ indicating that $x(t)$ influences rate of change $Y(t)$.
Apply the Riemann-Liouville Integral to operate I^a on both sides of the equation

$$(3.23) \quad I^a [D_\alpha[Y]] = I^a (R_1 Y(t) + x(t) R_2 Y(t))$$

Here we solve the fractional integral for Y

$$(3.24) \quad I = \int_0^\tau Y(\tau) d\tau = Y(t) - Y(0)$$

Substitute $Y(t) - Y(0)$ for I for the integral

$$(3.25) \quad Y(t) - Y(0) = I^a (R_1 Y(t) + x(t) R_2 Y(t))$$

Isolate $Y(t)$ to get the initial conditions

$$(3.26) \quad Y(t) = Y(0) + I^a (R_1 Y(t) + x(t) R_2 Y(t))$$

Define operator $G[Y(t)]$ which also belongs on the continuous function $C[0, \theta]$

$$(3.27) \quad G[Y(t)] = Y(0) + I^a (R_1 Y(t) + x(t) R_2 Y(t))$$

The solution of $Y(t)$ is a fixed point on the operator G , this satisfies certain properties like:

- Mapping into the space: $C[0, \theta]$ so that it operates within the continuous function and since $Y(0)$ and $I^a (R_1 Y(t) + x(t) R_2 Y(t))$ are continuous, the fractional integral I^a preserves continuity
- Contraction mapping: The operator G is a contraction under certain conditions meaning $\|G[Y_1(t)] - G[Y_2(t)]\| \leq L \|Y_1(t) - Y_2(t)\|$, with $L < 1$, which guarantees a unique solution where I^a represents the Riemann-Liouville fractional integral.

Consider two solutions $Y(t)$ and $Z(t)$ to analyze the difference between two trajectories:

$$(3.28) \quad G[Y(t)] - G[Z(t)] = I^a [R_1 (Y(t) - Z(t)) + R_2 (Y(t) - Z(t))]$$

Here we introduce the exponential decay factor and multiply both sides of the equation by e^{-nt} :

$$(3.29) \quad e^{-nt} [G(Y(t)) - G(Z(t))] = e^{-nt} I^a [R_1 (Y(t) - Z(t)) + R_2 (Y(t) - Z(t))]$$

Expand the fractional integral using the definition of the Riemann-Liouville fractional integral to replace I^a :

$$(3.30) \quad I^a [R_1 (Y(t) - Z(t)) + R_2 (Y(t) - Z(t))] = \frac{1}{\Gamma(\alpha)} \int_0^t (t-c)^{\alpha-1} [R_1 (Y(c) - Z(c)) + R_2 (Y(c) - Z(c))] dc$$

This formulation ensures that past values $f(c)$ contribute to the present state $f(t)$, weighted by $(t-c)^{\alpha-1}$, which scales historical influence.

Next, apply exponential decay within the integral multiplying by $e^{-n(t-c)}$:

$$(3.31) \quad \frac{1}{\Gamma(\alpha)} \int_0^t (t-c)^{\alpha-1} e^{-n(t-c)} [Y(c) - Z(c)] e^{-nc} [R_1 + uR_2] dc$$

Now introduce norm bound, it ensures that differences between solutions remain controlled over time

$$(3.32) \quad \|G[Y(t)] - G[Z(t)]\| \leq \frac{1}{\Gamma(\alpha)} \int_0^t (t-c)^{\alpha-1} e^{-n(t-c)} \|Y(t) - Z(t)\| [R_1 + uR_2] dc$$

Since norm properties allow a unique solution that depends on continuous initial conditions:

$$(3.33) \quad \|Y(c) - Z(c)\| \leq \|Y(t) - Z(t)\|,$$

when applying inequality (3.33) to inequality (3.32), we then factor $\|Y(t) - Z(t)\|$ out of the integral

$$(3.34) \quad \|G[Y(t)] - G[Z(t)]\| \leq (R_1 + uR_2) \|Y(t) - Z(t)\| \frac{1}{\Gamma(\alpha)} \int_0^t (t-c)^{\alpha-1} e^{-n(t-c)} dc$$

Now the integral evaluates to $\frac{\Gamma(\alpha)}{n^\alpha}$, we can substitute:

$$(3.35) \quad \|G[Y(t)] - G[Z(t)]\| \leq (R_1 + uR_2) \frac{1}{n^\alpha} \|Y(t) - Z(t)\|$$

so we can conclude:

$$(3.36) \quad \|G[Y(t)] - G[Z(t)]\| \leq (R_1 + uR_2) \frac{1}{n^\alpha} \|Y(t) - Z(t)\| \int_0^t \frac{\alpha-1}{\Gamma(\alpha)} dc$$

This bound ensures stability and controls deviations between trajectories.

Substituting the integral back into our expression because it is the definite integral of a constant independent of c , integrating from $[0, t]$:

$$(3.37) \quad \|G[Y(t)] - G[Z(t)]\| \leq (R_1 + uR_2) \frac{1}{n^\alpha} \|Y(t) - Z(t)\| \frac{\alpha-1}{\Gamma(\alpha)} t$$

This introduces a bounded scaling factor, which ensures a contraction effect.

Now we establish the contraction property and are observing the structure of the term:

$$(3.38) \quad \|G[Y(t)] - G[Z(t)]\| \leq (R_1 + uR_2) \frac{t}{n^\alpha \Gamma(\alpha)} \|Y(t) - Z(t)\|$$

Since the coefficient $\frac{t}{n^\alpha \Gamma(\alpha)}$ acts as a damping factor, it ensures:

$$(3.39) \quad \|G[Y(t)] - G[Z(t)]\| < \|Y(t) - Z(t)\|$$

The integral term accumulates past influences but remains bounded. The contraction property ensures that the operator G smooths out deviations over time. This proves that G satisfies a stability condition, meaning perturbations diminish rather than grow.

Since the operator $G[Y(t)]$ satisfies a contraction property, we guarantee the existence of a unique fixed solution, meaning:

$$(3.40) \quad G[Y(t)] = Y(t)$$

Thus, $Y(t)$ must satisfy the corresponding integral equation.

Formulation of Solution Using fractional calculus the Riemann-Liouville Integral, the solution is expressed in terms of the initial condition $Y(0)$ and the fractional integral I^α :

$$(3.41) \quad Y(t) = Y(0) + I^\alpha(R_1 Y(t) + x(t)R_2 Y(t))$$

where I^α represents memory-dependent contributions.

Expanding the solution form using fractional integral properties:

$$(3.42) \quad Y(t) = Y(0) + \frac{t^\alpha}{\Gamma(\alpha+1)}[R_1 Y(0) + x(0)R_2 Y(0)] + I^{\alpha+1}[R_1 Y'(t) + x'(t)R_2 Y(t) + x(t)R_2 Y'(t)]$$

- The first term $Y(0)$ captures the initial state
- The second term introduces memory scaling using Gamma function properties
- The third term accumulates past interactions via the fractional integral $I^{\alpha+1}$, ensuring long-term dependencies

Thus, the existence of a fixed point leads directly to the solution formulation

Operating equation (3.42) to the initial fractional order derivatives stated in equations (3.11)–(3.13):

$$(3.43) \quad x(t) = x(0) + \frac{t^\alpha}{\Gamma(\alpha+1)}[p_1 x(0)(1-qx(0)) - p_2 x(0)z(0)] + I^{\alpha+1}[p_1(1-2qx(t))x'(t) - p_2(z(t)x'(t) + x(t)z'(t))]$$

$$(3.44) \quad y(t) = y(0) + \frac{t^\alpha}{\Gamma(\alpha+1)}[x(0)z(0) + rd(t) - y(0) - sy(0)z(0)] + I^{\alpha+1}[x'(t)z(t) + x(t)z'(t) - y'(t) - sy'(t)z(t)]$$

$$(3.45) \quad z(t) = z(0) + \frac{t^\alpha}{\Gamma(\alpha+1)}[u(1-vz(0)) - x(0)z(0) - \delta y(0)z(0)] + I^{\alpha+1}[-vz'(t) - x'(t)z(t) - x(t)z'(t)]$$

Each population (N, L, T) now follows fractional-order memory dynamics, meaning past interactions influence current behavior. The Gamma function scaling ensures appropriate historical weighting, while the fractional integral term $I^{\alpha+1}$ allows for persistent effects in tumor-immune interactions. The system accounts for biological delays, making the model more realistic than classical differential equations.

3.2.2. Stability Analysis. Using the nondimensionalized model, we can solve for critical points and find $N_0 = L_0 = T_0 = 0$ for the trivial solution, and for non-zero values we have

$$(3.46) \quad N_i^* = \frac{p_1 - p_2 \pm \sqrt{4k_n p_1 q D(t) + p_1^2 - 2p_1 p_2 - 2p_1 T(t) + p_2^2 + 2p_2 T(t) + T^2(t)} - T(t)}{2p_1 q}$$

$$(3.47) \quad L_i^* = \frac{rD(t) + N(t)T(t)}{sT(t) + 1}$$

$$(3.48) \quad T_i^* = \frac{-\delta L(t) + u \pm \sqrt{\delta^2 L^2(t) - 2\delta u L(t) + 2\delta L(t)N(t) - 4k_t uv D(t) + u^2 - 2uN(t) + N^2(t)} - N(t)}{2uv}$$

and the Jacobian of the non-dimensionalized model is

$$J = \begin{bmatrix} -2p_1 q N(t) + p_1 - p_2 - T(t) & 0 & -N(t) & k_n \\ T(t) & -sT(t) - 1 & -sL(t) + N(t) & r \\ -T(t) & -\delta T(t) & -\delta L(t) - 2uvT(t) + u - N(t) & -k_t \\ 0 & 0 & 0 & 0 \end{bmatrix}$$

for the trivial case, the Jacobian becomes

$$J = \begin{bmatrix} p_1 - p_2 & 0 & 0 & k_n \\ 0 & -1 & 0 & r \\ 0 & 0 & u & -k_t \\ 0 & 0 & 0 & 0 \end{bmatrix}$$

This gives us the eigenvalues 0, $p_1 - p_2$, -1 , and u . Since u has a positive sign, -1 has a negative sign, and $p_1 - p_2$ could be positive or negative, we can conclude that the trivial case is a saddle point. For the case $L_0 = T_0 = D_0 = 0$, $N_0 = \frac{p_1 - p_2 + \sqrt{p_1^2 - 2p_1p_2 + p_2^2}}{2p_1q} = \frac{1}{q}$

$$J = \begin{bmatrix} -p_1 - p_2 & 0 & -\frac{1}{q} & k_n \\ 0 & -1 & \frac{1}{q} & r \\ 0 & 0 & u - \frac{1}{q} & -k_t \\ 0 & 0 & 0 & 0 \end{bmatrix}$$

This gives us the eigenvalues $-p_1 - p_2$ and -1 , which are negative, and $u - \frac{1}{q}$ which could be negative or positive. Since u and q are positive, $u - \frac{1}{q}$ will only be negative when $u < \frac{1}{q}$ or when $q < \frac{1}{u}$. So this set of initial conditions is a saddle point when $q > \frac{1}{u}$ (which corresponds with a NK population cap less than that of the tumor growth rate), and a stable sink when $0 < q < \frac{1}{u}$ (which corresponds with a NK population cap greater than that of the tumor growth rate).

Table 1: Eigenvalue results.

Parameters	Range	Eigenvalue	Stability
p_1	$(0, p_2)$	$p_2 - p_1 > 0$	unstable
p_1	(p_2, ∞)	$p_2 - p_1 < 0$	saddle point
p_2	(p_1, ∞)	$u + \frac{1}{q} \left(\frac{p_2}{p_1} - 1 \right) > 0$	unstable
q, p_2	$q \in \left(0, \frac{1}{u} \left(1 - \frac{p_2}{p_1} \right) \right)$ $p_2 \in (0, p_1)$	$u + \frac{1}{q} \left(\frac{p_2}{p_1} - 1 \right)$	NA

For $N = \frac{p_1 - p_2 - T(t)}{p_1q}$, $L = \frac{N(t)T(t)}{sT(t)+1}$, $T = \frac{u - N(t) - \delta L(t)}{uv}$, $D = 0$,

$$J = \begin{bmatrix} -p_1 + p_2 + \frac{z}{uv} & 0 & -\frac{p_1 - p_2 - \frac{z}{uv}}{p_1q} & k_n \\ \frac{z}{uv} & -\frac{sz}{uv} - 1 & -\frac{sz(p_1 - p_2 - \frac{z}{uv})}{p_1quv(\frac{sz}{uv} + 1)} + \frac{p_1 - p_2 - \frac{z}{uv}}{p_1q} & r \\ -\frac{z}{uv} & -\frac{\delta z}{uv} & 2\delta L(t) - \frac{\delta z(p_1 - p_2 - \frac{z}{uv})}{p_1quv(\frac{sz}{uv} + 1)} - u + 2N(t) - \frac{p_1 - p_2 - \frac{z}{uv}}{p_1q} & -k_t \\ 0 & 0 & 0 & 0 \end{bmatrix}$$

where $z = u - \delta L(t)$

4. Results. Our simulations produced a series of graphs that illustrated important aspects of immune cell dynamics and neuroblastoma tumor progression under various treatment conditions. These visualizations revealed critical trends, including the temporal changes in tumor growth and immune cell populations, and demonstrate the relative efficacy of Cyclophosphamide and IL-2 compared to the control groups. Notably, the combined therapeutic strategy approach consistently outperformed single-agent applications, highlighting the potential benefit of multi-drug treatment approaches.

4.1. Parameter selection. The initial conditions and parameters used in the model were informed by the interactions among tumor progression, drug concentration, and patient population, and were tailored to disease stage, with modifications adapted from the literature [5]. Our approach to modeling the immunotherapeutic dynamics of neuroblastoma was grounded in the International Neuroblastoma Risk Group (INRG) staging system [9], which significantly enhanced our ability to compare patient populations in the context of therapeutic interventions.

In this study, we employed a three category system to stratify patient populations into low, intermediate, and high-risk groups based on tumor stage (Table 1). This classification system supported the comparative analyses across trials and informed our initial conditions for the mathematical model. By aligning with an internationally accepted risk framework, we enhanced the clinical relevance and reproducibility of our simulations.

For each risk group, we estimated the relative initial abundances of tumor cells, CTLs, and NK cells, while paying particular attention to capturing the relative population sizes (Table 2). These immune profiles enabled a more accurate simulations of treatment outcomes under varying immunological baselines and allowed the exploration of how the immune system can influence therapeutic responses.

Table 2: Neuroblastoma disease stages defined by the International Neuroblastoma Risk Group.

Disease Stage	Description
Low Risk	Patients with L1 (localized tumors in one area) or MS (asymptomatic with favorable biology and metastases limited to skin, liver, or bone marrow) are considered low risk. These patients typically require observation, with surgery or chemotherapy only if symptoms arise.
Intermediate Risk	L2 (regional tumors with IDRFs) and MS with unfavorable biology (e.g., diploidy) are classified as intermediate risk. These tumors may need chemotherapy, with surgery recommended if possible.
High Risk	M (distant metastases), MS with MYCN amplification, or L2 in patients over 18 months with unfavorable features are high risk. These patients require aggressive treatment including chemotherapy, surgery, and stem cell therapy.

The low-risk population was characterized by a low tumor cell count and a highly active immune response, where NK cells, part of the innate immune system, offered immediate defense to tumor cells. While CTLs, which belong to the adaptive immune response, provided a targeted and more long-term defense with their abundance lower compared to NK cells. In the intermediate-risk population, the tumor cell count is higher, showing a more significant role for CTLs in the immune response. Though NK cells still serve as the first line of defense, the increased tumor burden necessitates a coordinated immune response, with CTLs becoming increasingly critical for targeting and eliminating the growing tumor cells. In the high-risk population, the tumor cell count is elevated, and the immune system faces greater challenges. While NK cells provided an early line of defense and gradually declined over time, CTLs proved to be essential for long-term tumor control. CTLs ability to recognize specific antigens and undergo clonal expansion enabled a sustained immune response against rapidly proliferating tumor cells.

Table 3: Pharmacology model parameters.

Parameter	Description	Units	Value
a_1	NK cell growth rate	$\text{cell} \cdot \text{day}^{-1}$	0.111
a_2	NK cell death rate due to natural death	day^{-1}	0.0412
b	Carrying capacity coefficient for NK cell population	cell^{-1}	1.02e-09
c	Natural tumor cell growth rate	day^{-1}	0.514
d	Carrying capacity coefficient for tumor cell population	cell^{-1}	1.02e-09
α_1	Rate of NK cell death due to tumor interaction	$\text{cell}^{-1} \cdot \text{day}^{-1}$	1e-07
α_2	Rate of NK-induced tumor death	$\text{cell}^{-1} \cdot \text{day}^{-1}$	3.23e-07
β_1	Rate of CTL-cell death due to tumor interaction	$\text{cell}^{-1} \cdot \text{day}^{-1}$	3.422e-10
β_2	Rate of CTL-induced tumor death	$\text{cell}^{-1} \cdot \text{day}^{-1}$	0.01245
μ	CTL cell death rate due to natural death	day^{-1}	0.02
r_1	Rate of NK-lysed tumor cell debris activation of CTLs	$\text{cell}^{-1} \cdot \text{day}^{-1}$	2.908e-11
k_c	Rate constant of Cyclophosphamide-mediated tumor death	$\text{mg}^{-1} \cdot \text{day}^{-1} \cdot \text{cell}$	0.9
k_i	Rate constant of IL-2-mediated stimulation	$\text{mg}^{-1} \cdot \text{day}^{-1} \cdot \text{cell}$	5e+04
h_i	Half-life of IL-2	day	–
h_c	Half-life of Cyclophosphamide	day	–
I_0	Dose of IL-2	mg	–
C_0	Dose of Cyclophosphamide	mg	–

Model parameters (Table 3) were selected to reflect biological processes driving neuroblastoma progression, immune system interactions, and the therapeutic effects of IL-2 and Cyclophosphamide. NK cell populations were regulated by intrinsic growth (a_1), death (a_2), and a carrying capacity constraint (b), while tumor-induced cytotoxicity was governed by the interaction rate (α_1). CTL dynamics were shaped by activation through NK-lysed tumor byproducts (r_1), natural cell death (μ), and tumor-induced depletion (β_1). Tumor proliferation was defined by the growth rate (c) and the carrying capacity (d), with immune-mediated reduction captured by NK and CTL-mediated lysis (α_2 , β_2).

Drug-related parameters chosen included the rate of IL-2 stimulation of NK cells (k_i) and the rate of Cyclophosphamide induced tumor reduction (k_c), both of which play important roles in modulating immune response and tumor growth in neuroblastoma. Their concentrations were modeled using first-order exponential decay based on pharmacokinetic half-lives (h_i , h_c), capturing the transient nature of these agents in systemic circulation. Initial dosages of IL-2 (I_0) and Cyclophosphamide (C_0) define the dosing schedule for treatment simulations (Table 3).

4.1.1. Pharmacological schedules. Dosing schedules for Cyclophosphamide and Interleukin-2 (IL-2) were differentiated by treatment intensity (low-dose and high-dose) and divided into initial and recurring administrations. For Cyclophosphamide, low-dose treatment involved an initial dose of 2.5 mg/kg followed by recurring doses of 2 mg/kg every 24 hours. High-dose treatment began with an initial dose of 30 mg/kg, with recurring doses of 25 mg/kg administered at 24-hour intervals [6]. IL-2 was administered on a fixed 24-hour cycle. Low-dose schedules involved an initial and recurring dose of 3×10^6 units, while high-dose schedules used 6×10^6 units per dose on the same interval [12].

Table 4: Dosing schedules for Cyclophosphamide and Interleukin-2.

Drug	Dosage	Initial	Recurring
Cyclophosphamide	Low	2.5 mg/kg	2 mg/kg
	High	30 mg/kg	25 mg/kg
IL-2	Low	–	3×10^6 units
	High	–	6×10^6 units

4.1.2. Therapeutic agent selection. Two therapeutic agents were selected for the modeling of neuroblastoma treatment: Cyclophosphamide and IL-2. These drugs were chosen for their complementary mechanisms in which they affect cellular populations. Cyclophosphamide acts through direct tumor cell cytotoxicity, whilst IL-2 enhances immune system activation and function. By incorporating both agents into our model, we aimed to quantify how chemotherapy induced tumor cell death and immune mediated tumor suppression independently and synergistically. This approach allowed for the exploration of direct cytotoxic effects and immune system activation across different stages of patient diseases.

Cyclophosphamide, a chemotherapy drug, directly targets tumor cells by slowing the rate at which they proliferate and inducing apoptosis. It chemically alkylates DNA, leading to the formation of crosslinks that interfere with replication and trigger cell death, in particular with rapidly dividing cells. Beyond its direct cytotoxicity, Cyclophosphamide controls the tumor microenvironment by suppressing immune responses [6]. Despite its effects, its potent ability to reduce tumor burden makes it a cornerstone in neuroblastoma treatment in modern medicine.

IL-2, an immune-modulating cytokine, plays a critical role in activation of NK cells, which are essential for the innate immune response against tumor cell development. IL-2 binds to receptors in NK cells, promoting proliferation, activation, and cytotoxicity. Activated NK cells then directly eliminate tumor cells by releasing perforin and granzymes, inducing apoptosis [14]. IL-2 enhances the expression of activating receptors in NK cells, improving their ability to recognize and target tumor cells, especially early on in the immune defense. In neuroblastoma treatment, this immune activation supports a shift toward a tumor-targeting immune environment [14].

4.2. Simulation of treatment strategies. Our analysis assessed various combinations of immunotherapy and chemotherapy across three distinct neuroblastoma patient populations stratified by risk level. Simulations were conducted to evaluate how treatment intensity and type influenced therapeutic outcomes within each group.

4.2.1. Low Risk. Low-risk simulations began with relatively small tumor populations and a partially functional immune system.

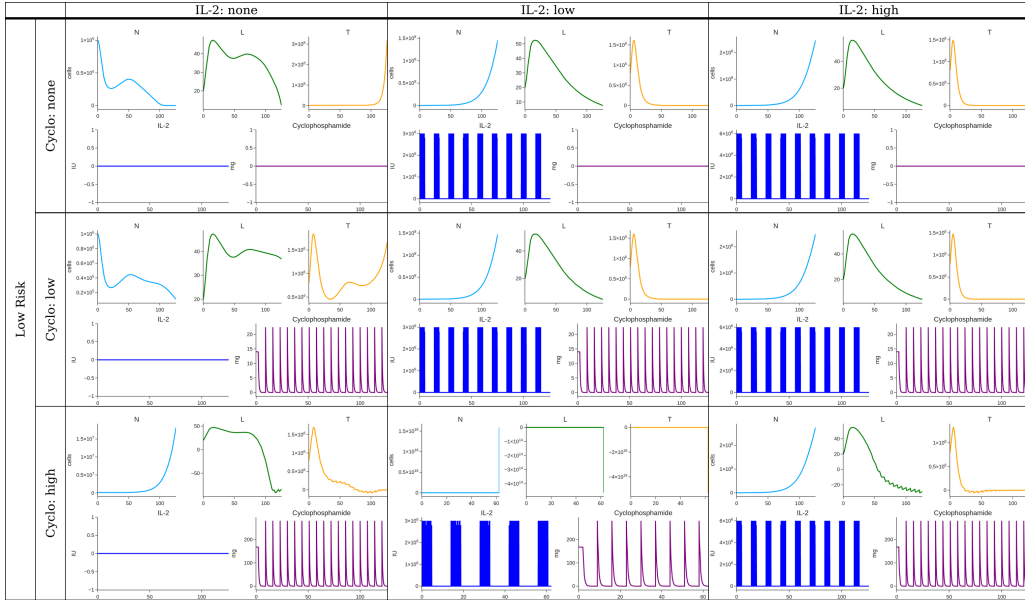


Fig. 1: Low-risk simulation results.

The results show in Fig. 1 shows either high doses of cyclophosphamide or low doses of interleukin-2 are necessary to overcome the tumor cells. Low doses of cyclophosphamide do temporarily decrease the amount of tumor cells, however as the tumor continues to grow it eventually outpaces the impact of the cyclophosphamide. Interleukin-2 is much more effective at suppressing the tumor through increasing NK cell production, and a low dose is sufficient. Simulations of combinations of interleukin-2 and high doses of cyclophosphamide with these initial conditions result in numeric instability as the tumor cell count becomes negative.

4.2.2. Intermediate-Risk. Intermediate-risk simulations were initialized with a higher tumor burden and a moderately suppressed immune response.

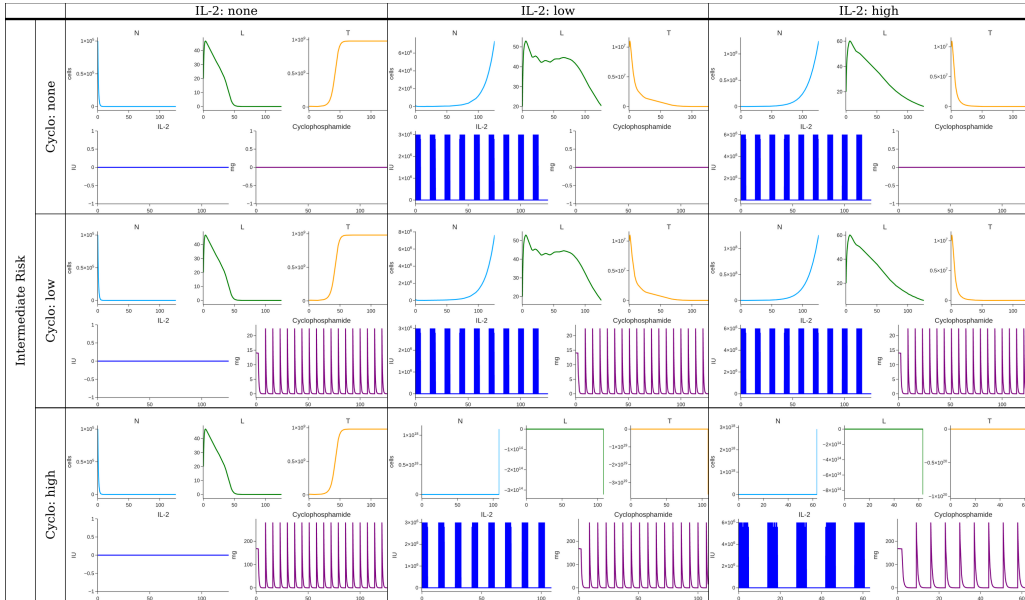


Fig. 2: Intermediate-risk simulation results.

The results show in Fig. 2 shows that administering interleukin-2 is necessary to overcome higher tumor burdens. Both low and high doses of cyclophosphamide are insufficient at this stage. Simulations where both interleukin-2 and high doses of cyclophosphamide are administered are numerically unstable, as the tumor cell count eventually becomes negative.

4.2.3. High-Risk. High-risk simulations were characterized by aggressive tumor growth and severely compromised immune cell populations.

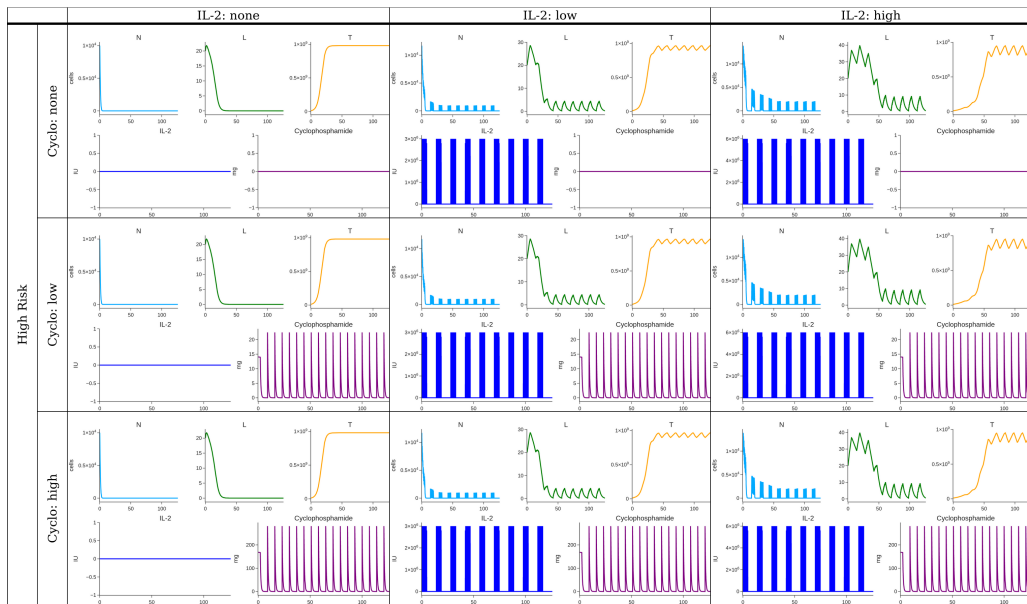


Fig. 3: High-risk simulation results.

The results show in Fig. 3 shows that no FDA approved combination of interleukin-2 and cyclophosphamide can suppress tumor cells in high risk conditions. Administering either low or high doses of cyclophosphamide result in no perceivable changes. Administering either low or high doses of interleukin-2 results in bursts of immune activity which are quickly overcome by the tumor cells.

Table 5: A matrix of the different simulation scenarios.

Risk	Cyclophosphamide Dose	IL-2 Dose		
		None	Low	High
Low	None	Low Risk No Cyclophosphamide No IL-2	Low Risk No Cyclophosphamide Low IL-2	Low Risk No Cyclophosphamide High IL-2
	Low	Low Risk Low Cyclophosphamide No IL-2	Low Risk Low Cyclophosphamide Low IL-2	Low Risk Low Cyclophosphamide High IL-2
	High	Low Risk High Cyclophosphamide No IL-2	Low Risk High Cyclophosphamide Low IL-2	Low Risk High Cyclophosphamide High IL-2
Intermediate	None	Intermediate Risk No Cyclophosphamide No IL-2	Intermediate Risk No Cyclophosphamide Low IL-2	Intermediate Risk No Cyclophosphamide High IL-2
	Low	Intermediate Risk Low Cyclophosphamide No IL-2	Intermediate Risk Low Cyclophosphamide Low IL-2	Intermediate Risk Low Cyclophosphamide High IL-2
	High	Intermediate Risk High Cyclophosphamide No IL-2	Intermediate Risk High Cyclophosphamide Low IL-2	Intermediate Risk High Cyclophosphamide High IL-2
High	None	High Risk No Cyclophosphamide No IL-2	High Risk No Cyclophosphamide Low IL-2	High Risk No Cyclophosphamide High IL-2
	Low	High Risk Low Cyclophosphamide No IL-2	High Risk Low Cyclophosphamide Low IL-2	High Risk Low Cyclophosphamide High IL-2
	High	High Risk High Cyclophosphamide No IL-2	High Risk High Cyclophosphamide Low IL-2	High Risk High Cyclophosphamide High IL-2

5. Conclusion. This study sought to examine the interactions between tumor cells, immune responses, and therapeutic agents in neuroblastoma using a system of coupled first-order ordinary differential equations. Our results emphasized and showed the crucial role NK cells and CTLs have in suppressing tumor growth and that both Interleukin-2 (IL-2) and Cyclophosphamide significantly enhance immune-mediated tumor elimination. IL-2 based tumor growth promoting NK cell proliferation and cytotoxic activity, while Cyclophosphamide exerted both direct tumor killing effects and immune stimulating properties. Simulations revealed that each treatment reduced tumor burden through distinct, complementary mechanisms.

By integrating immunotherapeutic and chemotherapeutic effects, our model highlighted the potential of combined drug therapies, providing valuable insights for treatment optimization strategies.

Data availability. Code and data used in this study is available on GitHub at: <https://github.com/JGarza189/neuroblastoma-2025>.

Acknowledgements. Our team extends sincere gratitude to Dr. BV Shankara Narayana Rao for her guidance and support throughout the project. Additionally, we would like to thank the Texas A&M High Performance Research Computing Group for portions of this research which were conducted with the advanced computing resources provided by Texas A&M High Performance Research Computing (HPRC).

REFERENCES

- [1] Anderson, J., Majzner, R. G., Sondel, P. M. (2022). Immunotherapy of neuroblastoma: Facts and hopes. *Clinical Cancer Research*, 28(15), 3196–3206.
- [2] Arceci, R. J. (2009). The International Neuroblastoma Risk Group (INRG) classification system: An INRG task force report. *Yearbook of Oncology*, 2009, 162–163.
- [3] Bellomo, N., Preziosi, L., Forni, G. (1997). Tumor immune system interactions: The kinetic cellular theory. *A Survey of Models for Tumor-Immune System Dynamics*, 135–186.
- [4] de Pillis, L. G., Gu, W., Radunskaya, A. E. (2006). Mixed immunotherapy and chemotherapy of tumors: Modeling, applications and biological interpretations. *Journal of Theoretical Biology*, 238(4), 841–862.
- [5] de Pillis, L., Fister, K. R., Gu, W., Collins, C., Daub, M., Gross, D., Moore, J., Preskill, B. (2008). Mathematical model creation for cancer chemo-immunotherapy. *Computational and Mathematical Methods in Medicine*, 10(3), 165–184.
- [6] Emadi, A., Jones, R. J., Brodsky, R. A. (2009b). Cyclophosphamide and cancer: Golden Anniversary. *Nature Reviews Clinical Oncology*, 6(11), 638–647.
- [7] Kuznetsov, V. A., Makalkin, I. A., Taylor, M. A., Perelson, A. S. (1994). Nonlinear Dynamics of immunogenic tumors: Parameter estimation and global bifurcation analysis. *Bulletin of Mathematical Biology*, 56(2), 295–321.
- [8] Loose, D., Van de Wiele, C. (2009). The immune system and cancer. *Cancer Biotherapy and Radiopharmaceuticals*, 24(3), 369–376.
- [9] Mueller, S., Matthay, K. K. (2009). Neuroblastoma: Biology and staging. *Current Oncology Reports*, 11(6), 431–438.
- [10] Padder, A., Almutairi, L., Qureshi, S., Soomro, A., Afroz, A., Hincal, E., Tassaddiq, A. (2023). Dynamical analysis of generalized tumor model with Caputo fractional-order derivative. *Fractal and Fractional*, 7(3), 258.
- [11] Postawa, K., Szczygieł, J., Kułazyński, M. (2020). A comprehensive comparison of ODE solvers for Biochemical Problems. *Renewable Energy*, 156, 624–633.
- [12] Pressey, J. G., Adams, J., Harkins, L., Kelly, D., You, Z., Lamb, L. S. (2016). In vivo expansion and activation of T cells as immunotherapy for refractory neuroblastoma. *Medicine*, 95(39).
- [13] Quaranta, V., Weaver, A. M., Cummings, P. T., Anderson, A. R. A. (2005). Mathematical modeling of cancer: The future of prognosis and treatment. *Clinica Chimica Acta*, 357(2), 173–179.
- [14] Rossi, A., Pericle, F., Rashleigh, S., Janiec, J., Djeu, J. (1994a). Lysis of neuroblastoma cell lines by human natural killer cells activated by interleukin-2 and interleukin-12. *Blood*, 83(5),
- [15] Roy, N. K., Bordoloi, D., Monisha, J., Anip, A., Padmavathi, G., Kunnumakkara, A. B. (2017). Cancer — an overview and molecular alterations in cancer. *Fusion Genes and Cancer*, 1–15.
- [16] Smith, V., Foster, J. (2018). High-risk neuroblastoma treatment review. *Children*, 5(9), 114.
- [17] Song, G., Liang, G., Tian, T., Zhang, X. (2022). Mathematical modeling and analysis of Tumor Chemotherapy. *Symmetry*, 14(4), 704.